HIGH-RESOLUTION UV LASER SPECTROSCOPY OF THE 1S2S3S1-]1SNP(N=5-79) TRANSITIONS IN HE-3 AND HE-4

Vassen, W.; Hogervorst, W.

published in
Physical Review A. Atomic, Molecular and Optical Physics
1989

DOI (link to publisher)
10.1103/PhysRevA.39.4615

document version
Publisher's PDF, also known as Version of record

High-resolution uv laser spectroscopy of the $1s2s\ ^3S_1 \rightarrow 1snp$ ($n=5-79$) transitions in ^{3}He and ^{4}He

Wim Vassen and Wim Hogervorst
Faculteit Natuurkunde en Sterrenkunde, Vrije Universiteit, De Boelelaan 1081, 1081 HV Amsterdam, The Netherlands
(Received 22 August 1988)

The ^{4}He fine structure and ^{3}He hyperfine structure as well as the isotope shift between ^{4}He and ^{3}He in the $1s2s\ ^3S_1 \rightarrow 1snp$ ($n=5$–79) transitions have been measured using an atomic beam and an intracavity frequency-doubled coumarin ring dye laser near 270 nm. The observed $1snp\ ^3P$ ^{4}He fine structure is in agreement with (extrapolations of) existing experimental results and theoretical calculations. The $1snp$ ^{3}He hyperfine structure has been analyzed using the ^{4}He fine-structure parametrization and the Fermi-contact interaction of the screened $1s$ electron. For $n>35$ hyperfine components of the $1snp\ ^1P$ levels are also excited as a consequence of hyperfine-induced singlet-triplet mixing. Calculated hyperfine splittings agree with experiment for $n<20$. Deviations up to 50 MHz are observed for $n>20$. These are shown to be due to hyperfine-induced n-mixing effects. The experimental results are excellently reproduced in a three-channel two-limit quantum-defect model without any adjustable parameter. The observed $1s2s\ ^3S_1 \rightarrow 1snp\ ^3P$ isotope shifts can be fully explained using recent mass polarization calculations for the $1s2s\ ^3S_1$ and $1snp$ ($n=3$–8) ^3P levels and confirm an isotope dependence of $\langle \mathbf{p}_1 \cdot \mathbf{p}_2 \rangle$ for the $1s2s\ ^3S_1$ level.

I. INTRODUCTION

Developments in high-resolution laser spectroscopy have facilitated extensive and detailed studies of bound Rydberg series of alkaline-earth atoms. These studies provide important information on configuration-interaction and correlation effects in two-electron systems.[1] The simplest two-electron system helium is also within reach of cw laser experiments although its bound Rydberg levels lie almost 200 000 cm^{-1} above the $1s^2\ ^1S_0$ ground state. Experiments on helium give the opportunity to study Rydberg series of two-electron systems below the first ionization limit in the absence of doubly excited configurations.

The fundamental nature of ^{4}He has stimulated many theoretical calculations and encouraged experimentalists to measure absolute level energies and fine-structure splittings with high accuracy. This has resulted in an excellent description of the low-lying ($n \leq 8$) levels of the $1snl$ ($l<5$) configurations.[2–4] Experiments on ^{4}He have been performed using excitations in low-pressure discharges or by electron bombardment in combination with microwave radiation (especially for D, F, and G states[5]) or with magnetic resonance methods.[6] By using one or two cw dye lasers low-lying S, P, and D levels have been studied in excitations from the $1s2s$ or $1s2p$ states.[7,8] In general these experiments were performed with discharges.

As ^{3}He has a nuclear spin ($I=\frac{1}{2}$) a detailed study of hyperfine interactions in the simplest two-electron atom is also possible. ^{3}He experiments have been reported for some S, P, and D states. In the ^3S series the levels $n=4$–6 (Ref. 9) and 12–14 (Ref. 10) and in the $^{1,3}D$ series $n=3$–6 (Ref. 9) and 12–17 (Ref. 11) have been investigated using two-photon ($n<7$) or two-step (via $5\ ^3P$) excitations from the $1s2s\ ^3S_1$ metastable level in a gas cell; the $1s3s\ ^3S_1$ level was studied in a discharge using a single red cw dye laser.[12] The ^3P series was investigated only for $n=2$,[13] 3,[14] and 5.[15,16]

Simultaneous study of ^{4}He and ^{3}He offers the possibility to observe the (large) isotope shifts. Isotope shift values for the $1s2s\ ^3S_1 \rightarrow 1sns\ ^3S_1$ ($n=4$–6),[17] $1s2s\ ^3S_1 \rightarrow 1snp\ ^3P_2$ [$n=2$ (Ref. 18), 5 (Ref. 19)], $1s2s\ ^3S_1 \rightarrow 1snd\ ^3D$ ($n=3$–6) (Refs. 17 and 20), and $1s5p\ ^3P_2 \rightarrow 1s13d$ (Ref. 19) transitions have been published. From these shifts the mass polarization of the levels involved may be deduced. Theory and experiment do not agree at the MHz level for the $1s2s\ ^3S_1$ and $1s5p\ ^3P$ states.[3,19]

In this paper we report the first high-resolution measurements of $1snp$ Rydberg levels with $n>8$ for both ^{4}He and ^{3}He. The experiments are performed in a beam of helium metastable atoms allowing field- and collision-free excitation. Theory and experimental setup are described in Secs. II and III, respectively. Results are presented and analyzed in Sec. IV. Conclusions are given in Sec. V.

II. THEORY

A. ^{4}He

The fine-structure splitting of the $1snp$ configuration of ^{4}He in $^1P_1$, $^3P_{0,1,2}$ levels may be described by the Hamiltonian

$$H_{\rm fs}=H_{\rm es}+H_{\rm s.o.}+H_{\rm s.o.o.}+H_{\rm s.s.}\ . \tag{1}$$

$H_{\rm es}$ is the electrostatic exchange interaction which, through the Slater exchange integral G, leads to the singlet-triplet splitting. $H_{\rm s.o.}$, $H_{\rm s.o.o.}$, and $H_{\rm s.s.}$ are the relativistic spin-orbit, spin-other-orbit, and spin-spin interactions resulting in the splitting of the ^3P levels ac-

cording to their J values ($J=0,1,2$). The relative strength of the interactions is determined by the spin-orbit parameter $\xi^{\text{s.o.}}$, the spin-other-orbit parameter $\xi^{\text{s.o.o.}}$, and the spin-spin parameter ψ. These relativistic interactions may be expressed as

$$H_{\text{s.o.}} = \mathbf{l}_2 \cdot \mathbf{s}_2 \xi^{\text{s.o.}} , \tag{2}$$

$$H_{\text{s.o.o.}} = -2\mathbf{l}_2 \cdot \mathbf{s}_1 \xi^{\text{s.o.o.}} , \tag{3}$$

$$H_{\text{s.s.}} = 2[\mathbf{s}_1 \cdot \mathbf{s}_2 - 3(\mathbf{s}_1 \cdot \mathbf{r}_{12})(\mathbf{s}_2 \cdot \mathbf{r}_{12})]\psi . \tag{4}$$

$\mathbf{l}_2$ and $\mathbf{s}_2$ are the orbital angular momentum and the spin of the Rydberg electron, $\mathbf{s}_1$ is the spin of the core electron ($\mathbf{l}_1 = \mathbf{0}$), and $\mathbf{r}_{12} = \mathbf{r}_2 - \mathbf{r}_1$, with $\mathbf{r}_1$ and $\mathbf{r}_2$ the position vectors of the electrons. Formulas (2), (3), and (4) are generalizations of formulas given by Chang for $1snl$ Rydberg series with $l \geq 2$.[4] Chang used $\xi^{\text{s.o.}} = \xi^{\text{s.o.o.}} = \psi$, derived with the Heisenberg approximation of a nonpenetrating Rydberg electron. The parameters $\xi^{\text{s.o.}}$ and $\xi^{\text{s.o.o.}}$ are related to the diagonal (D) and nondiagonal (N) spin-orbit parameters of Miller and Freund[6] via $\xi^{\text{s.o.}} = 2(D-N)$ and $\xi^{\text{s.o.o.}} = -(D+N)$. The nonzero matrix elements of H_{fs} in the $1snp$ SLJ-coupling scheme are

$$\begin{aligned}
&\langle 1snp\ ^1P_1 | H_{\text{fs}} | 1snp\ ^1P_1 \rangle = \tfrac{1}{2}G , \\
&\langle 1snp\ ^3P_0 | H_{\text{fs}} | 1snp\ ^3P_0 \rangle = -\tfrac{1}{6}G - (\xi^{\text{s.o.}} - 2\xi^{\text{s.o.o.}}) \\
&\qquad\qquad + 2\psi , \\
&\langle 1snp\ ^3P_1 | H_{\text{fs}} | 1snp\ ^3P_1 \rangle = -\tfrac{1}{6}G - \tfrac{1}{2}(\xi^{\text{s.o.}} - 2\xi^{\text{s.o.o.}}) - \psi , \\
&\langle 1snp\ ^3P_2 | H_{\text{fs}} | 1snp\ ^3P_2 \rangle = -\tfrac{1}{6}G + \tfrac{1}{2} \\
&\qquad\qquad \times (\xi^{\text{s.o.}} - 2\xi^{\text{s.o.o.}}) + \tfrac{1}{5}\psi , \\
&\langle 1snp\ ^3P_1 | H_{\text{fs}} | 1snp\ ^1P_1 \rangle = \tfrac{1}{2}\sqrt{2}(\xi^{\text{s.o.}} + 2\xi^{\text{s.o.o.}}) .
\end{aligned} \tag{5}$$

In the P series the exchange interaction dominates the relativistic interactions ($G \gg \xi^{\text{s.o.}}, \xi^{\text{s.o.o.}}, \psi$). As a result, singlet-triplet mixing is almost negligible, which explains why $1snp\ ^1P_1$ levels in ^{4}He cannot be excited from $1s2s\ ^3S_1$. The three relativistic parameters $\xi^{\text{s.o.}}$, $\xi^{\text{s.o.o.}}$, and ψ cannot be deduced independently from the splitting of the ^3P level alone. For this reason we set $\xi^{\text{s.o.}} = \xi^{\text{s.o.o.}} = \xi$. This assumption may not be true but there is no way to discriminate between $\xi^{\text{s.o.}}$ and $\xi^{\text{s.o.o.}}$, as the combination $\xi^{\text{s.o.}} - 2\xi^{\text{s.o.o.}}$ occurs in each diagonal matrix element of the ^3P_i levels [see Eq. (5)]. To obtain theoretical values for the ^{4}He fine structure as a function of the principal quantum number n scaling laws may be used. It is expected that all parameters (G, ξ, and ψ) scale as n^{-3} at high n.[2] To take into account deviations at low n ($n<8$), the fine-structure splittings are fitted with

$$f(n) = an^{-3} + bn^{-5} + cn^{-7} , \tag{6}$$

where higher odd powers are neglected, as they give only a small contribution for $n<4$. The fitting has been accomplished using experimental $^3P_1$-$^3P_0$ and $^3P_2$-$^3P_1$ splittings for $n=3$, 4, and 5 and $^1P_1$-$^3P_2$ separations calculated from the Rydberg-Ritz formulas for the $n\ ^1P$ and $n\ ^3P_2$ series.[2] From the resulting fit, G, ξ, and ψ may be calculated after diagonalization of H_{fs}. The result gives $\psi \approx 0.664\xi$ and $\xi \approx 1.0 \times 10^{-4} G$. Here G not only includes the exchange integral but also a contribution of the mass polarization [defined in Sec. III C, Eq. (9)]. From this parametrization it follows that the ^3P splittings decrease to the 10-MHz level around $n=20$ (see also Table I).

B. ^{3}He

To describe the hyperfine structure in the $1snp$ series of ^{3}He with $n \geq 5$ only one extra term needs to be added to the Hamiltonian H_{fs} [formula (1)], i.e., the Fermi contact interaction of the (screened) $1s$ electron

$$H_{\text{hfs}} = a_c \mathbf{I} \cdot \mathbf{s}_1 , \tag{7}$$

with a_c the Fermi contact parameter and $\mathbf{I}$ the nuclear spin ($I = \frac{1}{2}$). This extra term mixes states with different S and J since matrix elements of the type

$$\langle 1snp\ ^1P_1 F | H_{\text{hfs}} | 1snp\ ^3P_J F \rangle$$

TABLE I. Experimental (expt) and theoretical (theor) fine-structure splittings of $1snp\ ^3P_J$ for ^{4}He (in MHz). $^i\Delta^j$ is the energy difference between peaks with $J=i$ and $J=j$, whereas in $^{2,1}\Delta^0$ the center of gravity of the experimentally unresolved $J=1$ and $J=2$ peaks is accounted for.

n	$^2\Delta^1$(expt)	$^{2,1}\Delta^0$(expt)	$^1\Delta^0$(expt)	$^2\Delta^1$(theor)	$^{2,1}\Delta^0$(theor)	$^1\Delta^0$(theor)
5	134.9(7)		1661.5(6)	135.5		1661.9
6	75.6(40)		952.1(40)	77.3		951.5
7	46.5[a]		592.7[a]	48.2		595.2
8		418.3(30)		32.1	417.0	397.0
9		292.6(30)		22.4	292.0	277.9
10		214.2(30)		16.3	212.4	202.2
11		158.2(30)		12.2	159.3	151.6
12		122.9(30)		9.4	122.5	116.7
13		96.5(30)		7.4	96.3	91.7
14		75.8(30)		5.9	77.0	73.3
15		65.5(30)		4.8	62.6	59.6
17		42.7(30)		3.3	42.9	40.9
18		37.6(30)		2.8	36.2	34.4

[a]One spectrum recorded.

and

$$\langle 1snp\ ^3P_1 F | H_{\rm hfs} | 1snp\ ^3P_J F \rangle$$

are nonzero.

The parameter a_c is expected to approach its value in the ground state of the He^+ ion, i.e., -8665.65 MHz (Ref. 21) as with increasing n the hyperfine structure in the Rydberg series converges to the corresponding splitting of this ground state. Terms which depend on the np electron may be neglected. This is justified, as contributions of these terms are expected to decrease with n^3 and calculations for $n=5$ show a contribution of only about 1 MHz.[16] Diagonalization of the total Hamiltonian $H_{\rm fs}+H_{\rm hfs}$ results in seven hyperfine components with total angular momentum $F=\frac{1}{2}$ (three components), $F=\frac{3}{2}$ (three components), and $F=\frac{5}{2}$. The $1s2s\ ^3S_1$ level is split by the hyperfine interaction into two levels $F_g=\frac{1}{2}$ and $F_g=\frac{3}{2}$; the $F_g=\frac{1}{2}$ hyperfine level has highest energy and is separated from the $F_g=\frac{3}{2}$ level by 6739.70 MHz.[22] In the energy scheme shown in Fig. 1 the 13 possible transitions are indicated. However, four transitions are to the two hyperfine levels of ^1P and are forbidden as long as the total spin S is a good quantum number. From the remaining nine transitions four are predicted to have negligible intensity as follows from simple angular momentum algebra. This leaves five peaks which may be observed in an experiment: two excited from $F_g=\frac{1}{2}$ and three from $F_g=\frac{3}{2}$ (see Fig. 1). With increasing n these five peaks form two groups, each related to a specific ^3S hyperfine level. The splitting within each group approximately follows the ^{4}He ^{3}P splittings. For high n the ^1P-^3P separation, which scales as n^{-3}, becomes comparable with the hyperfine splittings of ^3P ($G\approx a_c$). Then S is no longer a good quantum number and hyperfine structure of "^1P" may be excited (see Fig. 1).

For an accurate calculation the G value deduced for ^{4}He has to be adjusted slightly to fit the ^{3}He hyperfine

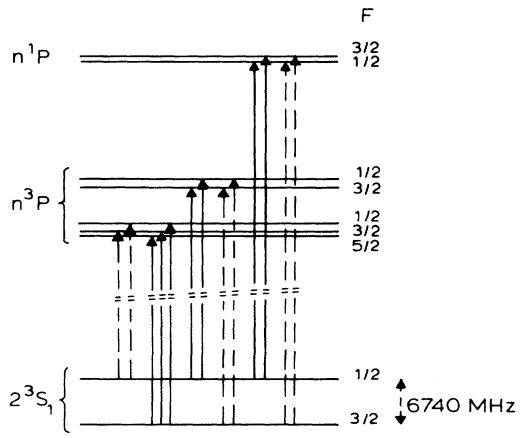

FIG. 1. Hyperfine structure of the $1s2s\ ^3S_1$ and $1snp$ states in ^{3}He. Solid lines indicate the strongest transitions. Dotted lines have negligible intensity. Transitions to ^1P are allowed for high n when the total spin S is no longer a good quantum number. Levels are labeled with their total angular momentum F.

structure:

$$G(^3\mathrm{He}) \approx 1.000\,44\, G(^4\mathrm{He})\ .$$

This accounts for an isotope dependence of the ^1P-^3P splitting.[23] The seven hyperfine level energies deduced from the diagonalization are tabulated in Table II relative to the $F=\frac{5}{2}$ level. For high n, contributions of the $1s(n\pm1)p$ configurations may no longer be neglected as the separation between neighboring Rydberg states becomes comparable to a_c. The incorporate these n-mixing effects multichannel quantum defect theory (MQDT) is applied.[1,24]

n mixing and MQDT

MQDT commonly deals with mutually interacting Rydberg series converging to different ionization limits. It provides a parametrization of energies and wave functions of perturbed Rydberg series and is capable of describing autoionization line profiles.[1] The essence of MQDT is the separation of long- and short-range interactions between a Rydberg electron and its ion core. At large distance the electron moves in a Coulomb field and may be described with Coulomb radial wave functions. Short-range interactions are accounted for with eigenquantum-defects μ_α and matrix elements $U_{i\alpha}$ describing the change in angular momentum coupling of the electron with the ion core when their distance increases. The close-coupling channels α reflect these interactions with the ion core, whereas the collision channels i correspond to the dissociated system. The parameters $\mu_\alpha, U_{i\alpha}$ and the energy differences between the ionization limits involved completely determine the energies and wave functions of all Rydberg levels (and continua) with a given total angular momentum value. As MQDT describes Rydberg series as a whole (channels) it is often superior to conventional analyses based on one-electron configurations and perturbation theory.

In helium doubly excited states lie far above the $1s$ ionization limit and consequently the $1snl$ Rydberg series are unperturbed in the usual sense. In ^{3}He, however, hyperfine interactions induce a splitting of the $1s$ ionization limit (or the He^+ ground state). Therefore two ionization limits exist: one (with hyperfine quantum number $F_c=1$) at energy $E=0$ and one (with $F_c=0$) at $E=+8665.65$ MHz. In this case MQDT may also be applied, as was recently shown by Sun and Lu[24] in the case of n-mixing effects in the hyperfine structure of the $5sns$ Rydberg series of ^{87}Sr (for $n>100$). To characterize the i and α channels for each total angular momentum F of the ^{3}He atom different coupling schemes are necessary. The collision channels i, corresponding to the dissociated system $He^+ + e$, are $(Is)j_2$ coupled: the He^+ ion consisting of a $1s$ electron ($s_1=\frac{1}{2}$) and a nucleus with nuclear spin ($I=\frac{1}{2}$) coupled together to $F_c=0$ or 1 ($\mathbf{F}_c=\mathbf{I}+\mathbf{s}_1$) and the Rydberg electron np with $j_2=\frac{1}{2}$ or $\frac{3}{2}$. The close-coupling channels α are determined by interactions in the core region and are therefore (almost) purely $(LS)I$ coupled. The $U_{i\alpha}$ matrix is consequently the $(Is)j_2$-$(LS)I$ transformation matrix which can be calculated in a

TABLE II. Calculated hyperfine structure energies (in MHz) relative to the $F=\frac{5}{2}$ components for the ^{3}He $1snp$ configuration from diagonalization of the total Hamiltonian (1) and (7).

n \ F	$\frac{5}{2}$	$\frac{3}{2}$	$\frac{1}{2}$	$\frac{3}{2}$	$\frac{1}{2}$	$\frac{1}{2}$	$\frac{3}{2}$
5	0.0	112.2	1141.8	6511.1	7281.9	4 253 418.7	4 253 421.7
6	0.0	64.1	679.2	6505.4	6922.1	2 466 325.8	2 466 328.8
8	0.0	26.6	291.2	6490.0	6657.4	1 042 487.6	1 042 490.6
9	0.0	18.6	205.1	6482.6	6599.5	732 784.5	732 787.5
10	0.0	13.5	149.7	6474.3	6559.6	534 720.4	534 723.4
11	0.0	10.1	112.5	6464.7	6529.1	402 222.5	402 225.5
12	0.0	7.8	86.7	6453.4	6503.6	310 268.3	310 271.7
13	0.0	6.1	68.2	6440.3	6480.2	244 470.6	244 473.6
14	0.0	4.9	54.6	6424.9	6457.5	196 157.4	196 160.4
15	0.0	4.0	44.4	6407.2	6434.2	159 890.2	159 893.2
17	0.0	2.7	30.5	6363.4	6382.9	110 550.2	110 553.2
19	0.0	1.9	21.9	6306.6	6321.5	79 871.7	79 874.7
20	0.0	1.7	18.7	6272.7	6285.8	68 840.9	68 844.0
22	0.0	1.3	14.1	6191.6	6202.2	52 384.5	52 387.6
24	0.0	1.0	10.8	6090.4	6099.3	41 010.1	41 013.3
26	0.0	0.8	8.5	5965.5	5973.2	32 923.8	32 927.0
28	0.0	0.6	6.8	5813.0	5819.9	27 046.7	27 049.9
30	0.0	0.5	5.5	5629.4	5635.6	22 703.4	22 706.6
35	0.0	0.3	3.5	5020.5	5025.4	16 025.5	16 028.6
40	0.0	0.2	2.3	4235.9	4239.7	12 721.1	12 723.6
45	0.0	0.1	1.6	3418.4	3421.1	11 069.3	11 071.2
51	0.0	0.1	1.1	2576.3	2578.1	10 088.1	10 089.3
60	0.0	0.1	0.7	1692.6	1693.7	9428.3	9429.0
75	0.0	0.0	0.4	906.0	906.5	9016.4	9016.8
79	0.0	0.0	0.3	780.0	780.4	8961.0	8961.3

straightforward way. The eigen-quantum-defects μ_α may be deduced from ^{4}He fine-structure data.[24] Values have been taken from Martin[2] and are slightly adjusted to take into account the mass dependence of the singlet-triplet separation (mass polarization difference[23,27]). Also only a linear energy dependence for the μ_α parameters is used, equal for all ^3P_J channels. The MQDT parameters for the different F values are given in Table III. For $F=\frac{1}{2}$ and $F=\frac{3}{2}$ a three-channel two-limit analysis has to be performed and for $F=\frac{5}{2}$ a simple one-channel analysis. The resulting calculated energies are given in Table IV relative to the $1snp$ $F=\frac{5}{2}$ level.

C. Isotope shift

Isotope-shift measurements in helium provide a sensitive test for computed wave functions. The P series are especially interesting, as here the specific mass shift (SMS) gives, in addition to the normal mass shift (NMS), large contributions to the observed isotope shift.

TABLE III. MQDT parameters for $1snp$ $F=\frac{1}{2}$, $\frac{3}{2}$, and $\frac{5}{2}$. Collision channels i are characterized by the pair (F_c, j_2) and I_i is given in MHz. $\mu_\alpha=\mu_\alpha^0+d\mu_\alpha/(n^*)^2$.

Parameter \ Channel	$F=\frac{1}{2}$ 1	2	3	$F=\frac{3}{2}$ 1	2	3	$F=\frac{5}{2}$ 1
α	$1snp\ ^1P_1$	$1snp\ ^3P_0$	$1snp\ ^3P_1$	$1snp\ ^1P_1$	$1snp\ ^3P_1$	$1snp\ ^3P_2$	$1snp\ ^3P_2$
i	$(1,\frac{3}{2})$	$(1,\frac{1}{2})$	$(0,\frac{1}{2})$	$(1,\frac{3}{2})$	$(1,\frac{1}{2})$	$(0,\frac{3}{2})$	$(1,\frac{3}{2})$
I_i	0	8665.65	8665.65	0	8665.65	8665.65	0
μ_α^0	−0.012 156 8	0.068 342 5	0.068 372 5	−0.012 156 8	0.068 372 5	0.068 375 0	0.068 375 0
$d\mu_\alpha$	0.007 45	−0.018 68	−0.018 68	0.007 45	−0.018 68	−0.018 68	−0.018 68
$U_{i\alpha}$	$\begin{vmatrix} \sqrt{8} & 0 & 2 \\ -1 & 3 & \sqrt{2} \\ -\sqrt{3} & -\sqrt{3} & \sqrt{6} \end{vmatrix}$	$1/\sqrt{12}$		$U_{i\alpha}$	$\begin{vmatrix} \sqrt{10} & \sqrt{5} & 3 \\ -\sqrt{8} & 4 & 0 \\ -\sqrt{6} & -\sqrt{3} & \sqrt{15} \end{vmatrix}$	$1/\sqrt{24}$	

TABLE IV. Calculated hyperfine-structure energies (in MHz) in the $1snp$ series of ^{3}He relative to the $F=\frac{5}{2}$ components with the three-channel two-limit MQDT model (for $J=\frac{1}{2}$ and $\frac{3}{2}$).

n \ F	$\frac{5}{2}$	$\frac{3}{2}$	$\frac{1}{2}$	$\frac{3}{2}$	$\frac{1}{2}$	$\frac{1}{2}$	$\frac{3}{2}$
5	0.0	113.8	1133.8	6517.2	7278.4	4 255 645.0	4 255 645.1
6	0.0	65.5	676.9	6505.7	6918.2	2 466 898.1	2 466 898.1
8	0.0	27.4	271.1	6490.9	6655.6	1 042 540.0	1 042 540.0
9	0.0	19.2	205.1	6483.8	6598.0	732 798.6	732 798.6
10	0.0	14.0	149.7	6475.7	6558.2	534 721.2	534 721.3
11	0.0	10.5	112.5	6466.3	6527.9	402 218.9	402 218.9
12	0.0	8.0	86.7	6455.3	6502.6	310 263.4	310 263.4
13	0.0	6.3	68.2	6442.5	6479.5	244 465.5	244 465.5
14	0.0	5.1	54.6	6427.5	6457.1	196 152.6	196 152.6
15	0.0	4.1	44.3	6410.1	6434.1	159 885.5	159 885.5
17	0.0	2.8	30.5	6367.3	6383.7	110 545.8	110 545.8
19	0.0	2.0	21.8	6311.7	6323.5	79 866.7	79 866.7
20	0.0	1.7	18.7	6278.5	6288.5	68 835.8	68 835.8
22	0.0	1.3	14.0	6199.1	6206.6	52 378.3	52 378.2
24	0.0	1.0	10.8	6100.0	6105.7	41 002.2	41 002.1
26	0.0	0.8	8.5	5977.7	5982.1	32 913.7	32 913.6
28	0.0	0.6	6.8	5828.3	5831.8	27 033.8	27 033.7
30	0.0	0.5	5.6	5648.1	5650.9	22 687.3	22 687.2
35	0.0	0.3	3.5	5048.8	5050.4	15 999.9	15 999.6
40	0.0	0.2	2.3	4272.2	4273.1	12 687.2	12 686.9
45	0.0	0.2	1.7	3458.4	3458.9	11 031.1	11 030.8
51	0.0	0.1	1.1	2617.0	2617.3	10 048.5	10 048.2
60	0.0	0.1	0.7	1732.8	1732.9	9388.6	9388.3
75	0.0	0.0	0.4	949.9	949.9	8971.6	8971.5
79	0.0	0.0	0.3	827.8	827.9	8911.4	8911.3

The isotope shift results from the difference in mass and volume of the nuclei of the isotopes involved. For a light element such as helium the volume shift is negligible. The observed isotope shift in a transition is then the sum of the NMS, which is the reduced-mass correction and may be calculated accurately, and the SMS. The NMS $\delta\nu^{4,3}$(NMS) for ^{4}He and ^{3}He is calculated from[20]

$$\delta\nu^{4,3}(\mathrm{NMS})=Em_e(M_4-M_3)/[M_4(M_3+m_e)] \ . \quad (8)$$

E is the ^{4}He energy difference in the transition. In the present work $E=E(n\,^3P_2)-E(2\,^3S_1)$, M_4 and M_3 are the nuclear masses of ^{4}He and ^{3}He ($M_4=4.001\,506\,079$ amu, $M_3=3.014\,932\,149$ amu), and $m_e=5.485\,803\times10^{-4}$ amu is the electron mass. These values have been taken from Wapstra and Audi.[26] The NMS calculated in this way differs by ~1.5 MHz from calculations published elsewhere;[17–19] the origin of this difference is unclear. The SMS is determined by $\mathbf{p}_1\cdot\mathbf{p}_2$ ($\mathbf{p}$ is the electron momentum vector) and is therefore a measure of electron correlation effects in the atomic wave function. SMS may be calculated from mass polarization (ϵ_m) calculations in ^{4}He using the mass dependence of ϵ_m. Generally[3,17,19,23,27] ϵ_M is expressed as

$$\epsilon_M=(m_e/M)\langle\mathbf{p}_1\cdot\mathbf{p}_2\rangle \ . \quad (9)$$

Theoretical values for the SMS in the $1s2s\,^3S_1\rightarrow1snp\,^3P_2$ transitions in ^{4}He have been evaluated from variational calculations of Kono and Hattori[3] for $n\leq8$. Especially for the higher $1snp$ levels their accuracy is much higher than that attained by Accad.[27] Assuming no mass dependence of $\langle\mathbf{p}_1\cdot\mathbf{p}_2\rangle$ the SMS for each level may be calculated directly from $\epsilon_{M=4}(M_4-M_3)/M_3$. For the $1s2s\,^3S_1$ this gives 2196.400 MHz and for the $1snp\,^3P_2$ levels of interest here -1124.71 MHz ($n=5$), -644.67 MHz ($n=6$), and -268.87 MHz ($n=8$); the error in the calculation is in the last digit. To obtain $1so$ values for $n>8$ the $n=3$–8 calculations are fitted with (6) and extrapolated. Results are given in column 5 of Table V.

Recent theoretical calculations of Drake[25] for the $1s^2$ and $1s2s$ levels in H^- and He using the mass polarization operator $(\mu/M)\mathbf{p}_1\cdot\mathbf{p}_2$ [μ is the reduced electron mass $m_eM/(m_e+M)$] show a small mass dependence of $\langle\mathbf{p}_1\cdot\mathbf{p}_2\rangle$:

$$\epsilon_M(1s2s\,^3S_1)=[1633.135\,00(\mu/M)-12\,617(\mu/M)^2]\ \mathrm{cm}^{-1} \ . \quad (10)$$

From this formula the SMS of the $1s2s\,^3S_1$ level is calculated as 2190.29 MHz, the 6-MHz difference from the value of 2196.400 MHz deduced from Kono and Hattori being almost entirely due to the quadratic term in (10).

TABLE V. Experimental and theoretical isotope shifts between ^{3}He and ^{4}He in the $1s2s\ ^3S_1 \rightarrow 1snp\ ^3P_2$ transition (in MHz). $\delta\nu^{4,3}$(TIS) is the transition isotope shift (measured frequency difference corrected for the ^{3}He hyperfine structure); the error is one standard deviation. $\delta\nu^{4,3}$(NMS) is the normal mass shift and $\delta\nu^{4,3}$(RIS)$=\delta\nu^{4,3}$(TIS)$-\delta\nu^{4,3}$(NMS) is the residual isotope shift. $\delta\nu^{4,3}(\mathrm{SMS}_{\mathrm{theor}})$ is the theoretical specific mass shift (deduced from Ref. 3). $\Delta=\delta\nu^{4,3}(\mathrm{RIS})-\delta\nu^{4,3}(\mathrm{SMS}_{\mathrm{theor}})$.

n	$\delta\nu^{4,3}$(TIS) (MHz)	$\delta\nu^{4,3}$(NMS)	$\delta\nu^{4,3}$(TIS)	$\delta\nu^{4,3}(\mathrm{SMS}_{\mathrm{theor}})$	Δ
5	48 961.2(40)	45 643.9	3317.3(40)	3320.6	−3.3
6	50 350.6(50)	47 515.7	2834.9(50)	2840.9	−6.0
8	51 822.8(30)	49 363.2	2459.6(30)	2465.5	−5.9
9	52 238.1(30)	49 858.9	2379.2(30)	2384.8	−5.6
11	52 768.1(50)	50 473.7	2284.4(50)	2299.2	−4.8
12	52 940.6(30)	50 671.9	2268.7(30)	2275.5	−6.8
13	53 076.4(30)	50 826.0	2250.4(30)	2258.5	−8.1
14	53 185.9(30)	50 948.1	2237.8(30)	2246.1	−8.3
15	53 272.7(30)	51 046.5	2226.2(30)	2236.7	−10.5
16	53 351.4(30)	51 127.0	2224.4(30)	2229.6	−5.2
17	53 411(5)	51 193.6	2217(5)	2224.1	−7
19	53 508.0(30)	51 296.6	2211.4(30)	2216.2	−4.8
20	53 543.0(30)	51 336.9	2206.1(30)	2213.3	−7.2
22	53 601.2(30)	51 401.5	2199.7(30)	2209.1	−9.4
24	53 648.1(30)	51 450.6	2197.5(30)	2206.2	−8.7
26	53 689.7(30)	51 488.9	2200.8(30)	2204.0	−3.2
28	53 710.0(30)	51 519.1	2190.9(30)	2202.5	−11.6
30	53 743.9(30)	51 543.6	2200.3(30)	2201.3	−1.0
35	53 778.9(30)	51 587.3	2191.6(30)	2199.5	−7.9
40	53 809.6(30)	51 615.7	2193.9(30)	2198.4	−4.5
45	53 827.7(30)	51 635.2	2192.5(30)	2197.8	−5.3
51	53 839.9(30)	51 651.4	2188.5(30)	2197.4	−8.9
60	53 856.6(30)	51 667.2	2189.4(30)	2196.9	−7.5
75	53 867.8(30)	51 682.0	2185.8(30)	2196.6	−10.8
79	53 872.7(30)	51 684.6	2188.1(30)	2196.5	−8.4

III. EXPERIMENTAL SETUP

The $1s2s\ ^3S_1 \rightarrow 1snp$ transitions in ^{3}He and ^{4}He are investigated using the laser–atomic-beam method. A thermal beam of metastable atoms is produced in a dc electric discharge running in an expanding helium gas. The beam source, schematically shown in Fig. 2, is based on the design of Fahey *et al.*[28] and consists of a quartz tube in which a stainless-steel needle cathode is inserted, a nozzle (0.2 mm diameter), and a stainless-steel cone-shaped skimmer with a 1-mm hole. A gas mixture of 50% ^{3}He and 50% ^{4}He at 50 Torr flows via an inlet valve into the quartz tube and expands through the nozzle into the vacuum chamber around the source. The dc discharge between the negative needle and the grounded skimmer runs at 13 mA, 0.6 kV and is simply initiated at high helium pressure using a ballast resistor of 75 kΩ in series with the discharge and a high ($\sim$2 kV) starting voltage. Although the metastable production is, in principle, linear with discharge current, higher currents have not been used due to fast degradation of the source at currents larger than 20 mA. The largest metastable fraction has been observed with a 10-mm nozzle-skimmer distance and 10^{-4} Torr in the source region (adjustable with the inlet valve). The nozzle orifice, originally at 0.2 mm, gradually widened during experiments resulting in increasing Doppler widths. Behind the skimmer a vacuum of $< 10^{-6}$ Torr is maintained in the excitation and detection chamber. To minimize the costs of the experiment the source region is part of a helium recycling system. A beam source of this kind produces in the order of 10^{14} metastable atoms per second per steradian with a thermal velocity of $\sim$2000 m/s.[28]

To reduce Doppler effects the metastable beam is collimated with an adjustable slit (0.3 mm, collimation ratio

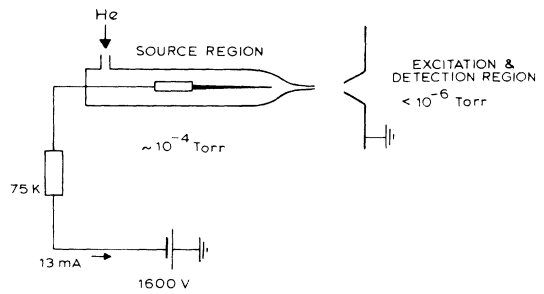

FIG. 2. Schematic of the metastable helium beam source.

1:600) and intersected perpendicularly with the focused laser light. The 90° angle is monitored by retroreflecting the light beam into the interaction region and observing the excitation profile. Laser radiation in the wavelength region 260–295 nm ($n=100\rightarrow 5$) has been produced by frequency doubling of a cw dye laser using various nonlinear crystals. The nonlinear crystals are inserted in the laser cavity and either angle tuned ($n=6,7$) or temperature tuned ($n=5,8$–75). In the temperature-tuned system a 20-mm long nonlinear crystal and a 20-mm long quartz compensating rhomb, both cut at Brewster angles for the visible are placed in the cavity of a frequency stabilized Spectra-Physics 380D ring dye laser.[29] The output coupling mirror is replaced by a high reflector transmitting only a small fraction of the visible light sufficient for stabilization and calibration purposes. The other mirror in the collimating arm is uv transparent ($\sim 70\%$). The nonlinear crystal is positioned in the auxiliary focus of the ring and temperature stabilized using a double-oven system which maintains the crystal at any temperature between room temperature and 110 °C.

To cover the region 260–295 nm three different types of nonlinear materials have been used. With a temperature-tuned 90° phase-matched ammonium dihydrogen arsenate (ADA) crystal inside a rhodamine 6G ring laser, uv radiation around 295 nm is generated for the excitation of the $1s5p$ levels. For $n=8$–17 ($\lambda=262.5$–272 nm) an ammonium dihydrogen phosphate (ADP) temperature-tuned crystal is used in a ring laser operating on the dye coumarin 6 [1.2 mmol/l, solvent of 40% benzyl alcohol and 60% ethylene glycol, with 6-g/l 9-methyl anthracene (additive A) added as triplet quencher]. With this crystal 14 mW of single-frequency uv radiation is produced near 270 nm with 8 W from an argon-ion laser at 488 nm. Although the half life of the coumarin dye is stated as 100 W-h, hardly any degradation of the output power is observed for at least 500 W-h, however, the stability of the output decreases gradually forcing dye change every 500 W-h. The use of the ADP crystal is limited to wavelengths above 262.5 nm. To study Rydberg levels with $n>18$ ($\lambda=260$–262.5 nm) the small-temperature coefficient of potassium dihydrogen phosphate (KDP) enables 90° phase matching for this range. As the 520–525-nm region is close to the edge of the useful range of coumarin 6 dye, uv power is typically 3 mW here. No crystal damage due to the high circulating power is observed. The wavelengths $\lambda=283$ and 276 nm ($n=6,7$) have been produced in a 10-mm-long angle-tuned KDP crystal, also positioned in the focus of the ring laser. The linewidth of the uv laser radiation is around 1 MHz and scans of 60 GHz are possible for both the angle- and temperature-tuned systems.

The helium Rydberg atoms are detected using two different methods. For $n<10$ fluorescence is observed with a photomultiplier. The lifetime of the $1snp$ Rydberg atoms varies from 0.2 to 1.0 μsec for $n=5$ and 10,[30] which is sufficiently short to detect fluorescence photons before the atoms leave the light-collecting lens system. For $n\geq 10$ the signals from the photomultipier are too weak and Rydberg atoms are ionized and detected with an electron multiplier. In earlier experiments on barium we detected the detached electrons;[31] this technique was not feasible in the case of helium due to the presence of large background signals. This background may be caused by secondary electrons produced by collisions of metastable helium atoms with metal surfaces. These electrons are emitted with 15-eV kinetic energy with a yield as high as 50% for stainless steel.[32] For this reason He^+ ions are detected with a quadrupole mass filter. To ensure field-free excitation the atomic and laser beam intersect in a metal shielding box. This box is kept at about +20 V. Rydberg atoms leaving this box pass a narrow gap of 1 mm width (distance ~ 0.5–1.5 cm from the interaction region) and enter the shielded quadrupole mass filter. The Rydberg atoms are ionized either by the 200 V/cm field or by blackbody radiation and the ions are accelerated into the quadrupole. Electrostatic lenses at the exit of the quadrupole focus the selected ions on an electron multiplier. The signal is further processed with a counting system and stored on a minicomputer which also controls the laser scan.

The transmission of part of the visible output of the ring laser through a length-stabilized étalon is also stored on the minicomputer for calibration purposes. The free spectral range (FSR) of 148.9568 MHz for this étalon is determined with an accuracy better than 1 kHz by measuring the sodium D_1 and D_2 lines [frequency difference 17.195 91 (6) cm^{-1} (Ref. 33)] with respect to Fabry-Pérot fringes locking the étalon to an iodine-stabilized He-Ne laser. This He-Ne laser is also used as a reference for wavelength measurments with a fringe-counting Michelson interferometer (absolute accuracy 100 MHz). The experimental setup is schematically shown in Fig. 3.

IV. RESULTS AND ANALYSIS

A. Fine and hyperfine structure

Examples of excitation spectra $1s2s\ ^3S_1\rightarrow 1snp$ are shown in Figs. 4 and 5. Each spectrum took about five

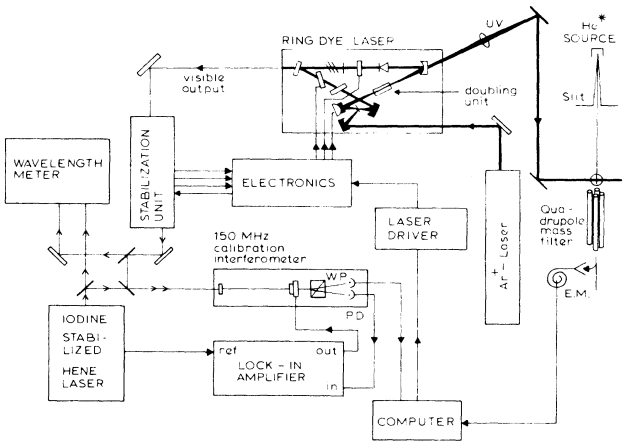

FIG. 3. Schematic of the experimental setup: WP, Wollaston prism; PD, photodiode; EM, electron multiplier.

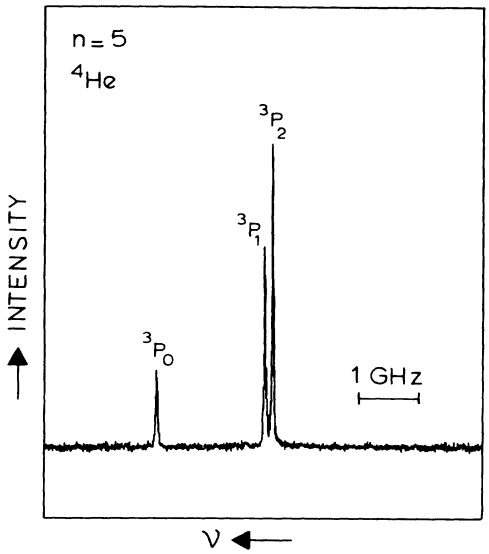

FIG. 4. Excitation spectrum $1s2s\ ^3S_1 \rightarrow 1s5p\ ^3P$ for ^{4}He at 295 nm. Levels are assigned according to their *LSJ* values.

minutes recording time and was recorded five times. The narrowest linewidth observed was 15 MHz full width at half maximum (FWHM). Even for high n values (up to $n=100$) this narrow linewidth was observed implying that effects of possible stray electric fields in the interaction region have been reduced efficiently to a level below a few mV/cm. In Fig. 4 a spectrum of $5\ ^3P$ of ^{4}He is shown. To record this spectrum, 3 mW uv power was used. Higher uv power was available but only resulted in saturation broadening of the transition. A background of 6000 counts/sec was almost entirely due to scattering of the uv light on the entrance and exit windows of the atomic beam apparatus. The splittings of the ^{4}He levels decrease as n^{-3}; as a result, $^3P_1$ and $^3P_2$ could not be resolved for $n>7$ and no splitting at all is observed for

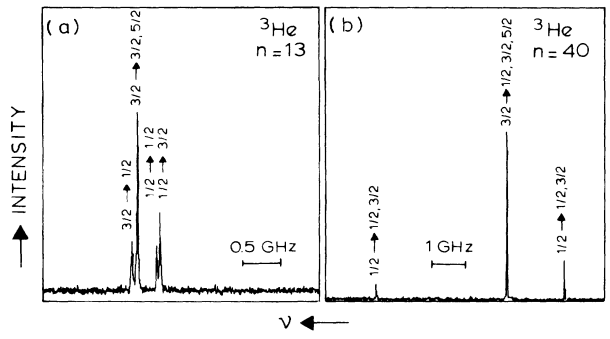

FIG. 5. Excitation spectra $1s2s\ ^3S_1 \rightarrow 1snp$ for $n=13$ [(a), $\lambda=263$ nm] and 40 [(b), $\lambda=261$ nm] for ^{3}He. Peaks are designated with the total angular momentum F of lower and upper state. Small peak at the left in (b) is the hyperfine-induced excitation of $^1P_1$.

$n>18$. Two examples of ^{3}He spectra are shown in Fig. 5. As indicated in Sec. II B the observed ^{3}He hyperfine structure contained five peaks for $n=5$ and 6, four for $n=8$–17, and only two for $n>18$. For $n>35$ one additional peak was observed as a consequence of hyperfine-induced singlet-triplet mixing. In Fig. 5(a) the hyperfine structure of the $1s2s\ ^3S_1 \rightarrow 1s13p\ ^3P$ transition is shown. The small separation between the two doublets reflects the near equality of the lower- and upper-state splitting (both ~ 6 GHz). Figure 5(b) shows the spectrum $1s2s\ ^3S_1 \rightarrow 1s40p\ ^{1,3}P$, where each peak is either a doublet or a triplet. The small peak at the high-frequency side is the hyperfine-induced ^1P excitation. The background in Fig. 5 (~ 500 counts/sec) and in all other spectra with $n \geq 10$ was always observed when the discharge was turned on. It is probably due to He^+ ions produced close to the electron multiplier via a process such as

$$He^* + e \rightarrow He^+ + 2e\ .$$

The electrons for this process are efficiently produced in metastable (He^*)-wall collisions.[32]

Although transition probabilities decrease with n^3, observed intensities for high n are comparable to or even larger than for low n. This is not only a consequence of the longer lifetime but may also be due to more efficient ionization of high-n Rydberg atoms. The primary mechanism for low-n ($n<25$) Rydberg atoms is direct ionization by blackbody radiation; the ionization rate for this process is estimated to be 10^4 sec^{-1}.[34] Field ionization is highly unlikely, as a field of 200 V/cm is far below the classical saddle-point field strength for such a process. Only for high n ($n>30$) may field ionization be expected to contribute significantly.

The splittings deduced from the ^{4}He and ^{3}He spectra are collected in Tables I [$^j\Delta^j = E(^3P_i) - E(^3P_j)$] and VI, respectively. All peaks are fitted with a symmetrical line profile. This may not be fully warranted in all cases as some peaks are doublets or even triplets. For ^{3}He the splittings as a function of n are shown in Fig. 6, relative to the single $F=\frac{5}{2}$ level. Clearly shown in energy and wave-function composition is the influence of the ^1P level as it approaches the ^3P levels. The negligible singlet-triplet mixing in the fine structure (^{4}He) results in the admixture of ^1P character only in two hyperfine components of ^3P (see Fig. 6). For some of the results given in Tables I and VI data are available in the literature. In Table VII a comparison of the present results and existing data is given. The ^{4}He splittings for $n=5$–8 were measured by several groups using different and sometimes more accurate methods.[6] For ^{3}He, only for $n=5$ can a comparison be made. All our data agree very well with literature values with two exceptions. The $5\ ^3P_2$-$5\ ^3P_1$ splitting as determined by Millar and Freund[6] deviates from the other values. The measurement of the $7\ ^3P_1$-$7\ ^3P_0$ interval of Wittmann *et al.*[6] is not in agreement with calculations as pointed out already by Martin.[2]

In Table I calculated ^{4}He splittings (see Sec. II A) are also given. For nonresolved peaks ($n \geq 8$) the center of gravity is also calculated and included in the table. Ex-

TABLE VI. Experimental ($F_{\text{expt.}}$) and theoretical ($F_{\text{theor.}}$) hyperfine-structure energies (in MHz) in the $1snp$ series of ^{3}He relative to the $F=\frac{5}{2}$ components. The error in the experimental values is one standard deviation in the distance to the $F=\frac{5}{2}$ level. Theoretical values are for $n<15$ averaged from Table II (diagonalization $1snp$) and for $n\geq 15$ from Table IV (MQDT).

	F_{expt}						F_{theor}					
n	$\frac{5}{2}$	$\frac{3}{2}$	$\frac{1}{2}$	$\frac{3}{2}$	$\frac{1}{2}$	$(\frac{1}{2}+\frac{3}{2})$	$\frac{5}{2}$	$\frac{3}{2}$	$\frac{1}{2}$	$\frac{3}{2}$	$\frac{1}{2}$	$(\frac{1}{2}+\frac{3}{2})$
5	0.0	115.7(30)	1145.7(30)	6513.7(30)	7284.3(30)		0.0	112.2	1141.8	6511.1	7281.9	4 253 420.7
6	0.0	57.3(40)	682.4(40)	6508.2(40)	6920.7(40)		0.0	64.1	679.2	6505.4	6922.1	2 466 327.8
8	0.0		282.1(30)	6479.3(30)	6643.7(30)		0.0		280.6	6479.4	6646.8	1 042 479.0
9	0.0		196.8(30)	6477.4(30)	6589.6(30)		0.0		197.7	6475.2	6592.1	732 779.1
10	0.0		143.5(30)	6470.1(30)	6556.7(30)		0.0		144.3	6468.9	6554.2	534 717.0
11	0.0		109.6(30)	6461.5(30)	6525.7(30)		0.0		108.5	6460.7	6525.1	402 220.5
12	0.0		84.8(30)	6451.5(30)	6500.7(30)		0.0		83.6	6450.3	6500.5	310 267.2
13	0.0		66.6(30)	6437.7(30)	6476.7(30)		0.0		65.8	6437.9	6477.8	244 470.2
14	0.0		52.7(30)	6421.7(30)	6451.2(30)		0.0		52.6	6422.9	6455.5	196 157.4
15	0.0		45.5(30)	6411.4(30)	6436.2(30)		0.0		42.7	6408.5	6432.5	159 883.9
17	0.0		29.9(30)	6363.8(30)	6381.5(30)		0.0		29.4	6366.2	6382.6	110 544.7
19		0.0		6311.5(30)			0.0			6314.8		79 865.9
20		0.0		6277.7(30)			0.0			6281.2		68 835.1
22		0.0		6200.1(30)			0.0			6200.9		52 377.6
24		0.0		6099.8(30)			0.0			6101.5		41 001.7
26		0.0		5977.6(30)			0.0			5978.8		32 913.4
28		0.0		5826.3(30)			0.0			5829.2		27 033.5
30		0.0		5646.3(30)			0.0			5648.8		22 687.0
35		0.0		5048.9(30)			0.0			5049.2		15 999.6
40		0.0		4271.2(30)		12 688.1(30)	0.0			4272.4		12 686.6
45		0.0		3454.5(30)		11 026.8(30)	0.0			3458.5		11 030.8
51		0.0		2612.5(30)		10 048.6(30)	0.0			2617.1		10 048.3
60		0.0		1731.7(30)		9387.6(30)	0.0			1732.8		9388.4
75		0.0				8970.5(30)	0.0			949.9		8971.5
79		0.0				8909.6(30)	0.0			827.8		8911.3

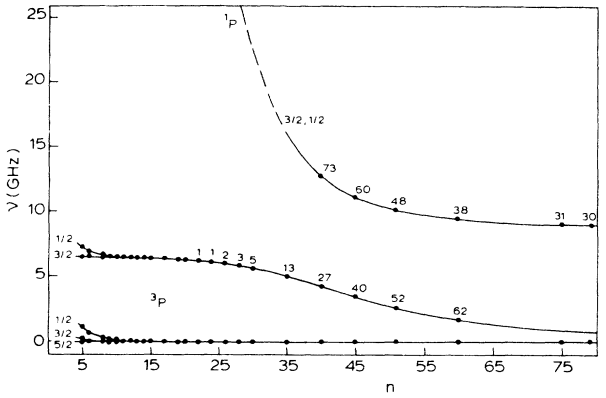

FIG. 6. Experimental hyperfine level energies of ^{3}He $1snp$ relative to the $F=\frac{5}{2}$ position as a function of n. For each hyperfine component the ^1P fraction in the wave function is as indicated or smaller than 1%.

periment and semiempirical theory show excellent agreement in this case.

In the ^{3}He spectra, where the triplet $\frac{5}{2},\frac{3}{2},\frac{1}{2}$ is not resolved ($n>17$) the center of gravity of only the $\frac{5}{2}$ and $\frac{3}{2}$ is calculated from theory as the weak transition to $F=\frac{1}{2}$ is ignored in the peak fitting routine. Only for $n=5$ is a theoretical parameter (a_c) fitted in the $1snp$ diagonalization procedure as the screening of the $1s$ electron by the $5p$ electron may reduce the value of a_c significantly. The best fit is obtained with $a_c=-8657$ MHz, which is 9 MHz below the He^+ ground-state splitting. For $n\geq 6$ fitting of a_c does not improve the results.

Comparison of the experimental results in Table VI and theoretical values in Table II obtained from the $1snp$ diagonalization procedure show that experiment and theory agree well up to $n=20$. For $n>20$ deviations increase with n and reach a maximum value of 50 MHz at $n=75$. These deviations obviously are due to n-mixing effects as follows from a comparison of the experimental values with the MQDT energies in Table IV. The observed hyperfine level energies are reproduced by MQDT for $n\geq 8$. For $n<15$ deviations between calculations of the singlet-triplet separation (Tables II and IV) are noteworthy, resulting from the use of only linear energy-dependent μ_α parameters in the MQDT model. The 3-MHz splitting within the $1snp$ $^1P_1$ level as given in Table II but not in Table IV is due to singlet-triplet mixing [off-diagonal matrix element in (5)] not included in the MQDT model (pure LS-coupled α basis). The deficiencies in the MQDT model may be solved by inclusion of higher-order energy dependence of the parameters and a small correction in the matrix $U_{i\alpha}$. In Table VI the theoretical results are compared with experiment using averaged values of Table II for $n<15$ and from Table IV for $n\geq 15$. Experiment and theory show excellent agreement.

B. Isotope shift

From spectra obtained in a ^{3}He-^{4}He gas mixture the frequency difference between the ^{4}He $^3P_2$ peak and the ^{3}He($\frac{3}{2}\rightarrow\frac{5}{2}$) peak was determined; the $^3P_2$ component was chosen because the $F=\frac{5}{2}$ of ^{3}He is a pure $J=2$ state. This frequency difference is approximately 50 GHz (the ^{4}He peak at higher frequency). Large scans are quite cumbersome to preform and not very accurate so they were made only as a check for a few n values ($n=5$, 17, and 30). A scan for $n=30$ is shown in Fig. 7. A more ac-

TABLE VII. Summary of experimental data on $1snp$ fine structure (^{4}He), hyperfine structure (^{3}He), and isotope shift [experimental separation ^{3}He($\frac{3}{2}\rightarrow\frac{5}{2}$)$-^4$He($^3S_1\rightarrow{}^3P_2$)]. All values are in MHz.

			Expt. data					
	n	Transition	This work	Miller and Freund[a]	Kaul[a]	Descoubes[a]	Wittmann *et al.*[a]	Bloomfield *et al.*[b]
^{4}He	5	$^3P_2$-$^3P_1$	134.9(7)	137.4(7)		135.5(1)	135.2(5)	134.3(1.0)
		$^3P_1$-$^3P_0$	1661.5(6)	1660.0(8)	1662.1(4)		1654(8)	
	6	$^3P_2$-$^3P_1$	75.6(4.0)			77.3(1)	75.0(2.0)	
		$^3P_1$-$^3P_0$	952.1(4.0)		950.0(6)		965(10)	
	7	$^3P_2$-$^3P_1$	46.5			48.4(2)	51.0(2.0)	
		$^3P_1$-$^3P_0$	592.7				574(4)	
^{3}He	5	$\frac{5}{2}$-$\frac{3}{2}$	115.7(3.0)			113.5(5)		113.5(1.0)
		$\frac{5}{2}$-$\frac{1}{2}$	1145.7(3.0)				1144.4(2.5)	
		$\frac{5}{2}$-$\frac{3}{2}$	6513.7(3.0)				6513.7(2.5)	
		$\frac{5}{2}$-$\frac{1}{2}$	7284.3(3.0)				7282.7(2.5)	
	6	$\frac{5}{2}$-$\frac{3}{2}$	57.3(4.0)			64.0(2)		
Isotope shift	5		48 878.9(3.0)					48 878.8(3.0)

[a]Reference 6.
[b]References 16 and 19.

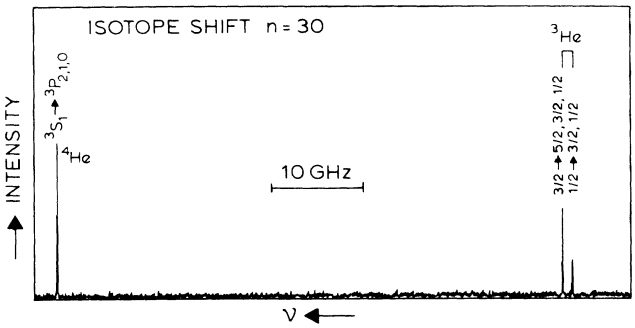

FIG. 7. Isotope shift between ^{4}He and ^{3}He in the $1s2s\ ^3S_1 \rightarrow 1s30p$ transition at 261 nm.

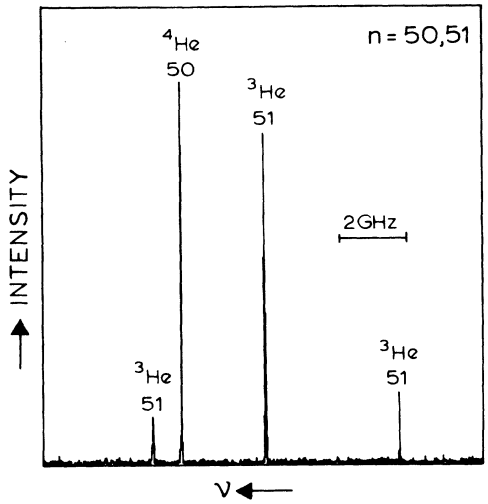

FIG. 8. Spectrum $1s2s\ ^3S_1 \rightarrow 1snp$ for $n=50$ in ^{4}He and $n=51$ in ^{3}He ($\lambda=260$ nm).

curate method to determine this separation is to measure the relevant peak positions relative to Fabry-Pérot fringes of the calibration interferometer. This gives the required separation when the FSR of the étalon is accurately known and the number of fringes between both peaks is known. The results of this procedure are collected in Table V. The quoted data are the result of five measurements of ^{4}He immediately followed by five ^{3}He spectra or vice versa; care has been taken not to change any alignment of laser and/or atomic beam as this might result in small additional Doppler shifts. Only one isotope-shift measurement is available from literature[19] ($n=5$); this measurement is in agreement with the present result (see Table VII).

A consequence of the large isotope shift is the near coincidence of the $1snp$ peak of ^{4}He with the $1s(n+1)p$ peaks of ^{3}He near $n=50$. This is shown in Fig. 8 where the ^{4}He $50p$ peak and the ^{3}He $51p$ hyperfine peaks are excited. This coincidence may be useful for a more accurate isotope-shift measurement, as the energy difference between $50p$ and $51p$ can be calculated accurately (<1 MHz error).[2] The $n=50$ isotope shift, given in Table V, has been determined in this way.

To derive the transition isotope shift (TIS) of the $1s2s\ ^3S_1 \rightarrow 1snp\ ^3P_2$ transition the measured separation has to be adjusted to account for the ^{3}He hyperfine structure. The center of gravity of the $^3S_1 \rightarrow {}^3P_2$ transition in ^{3}He may be derived from the measured $\frac{3}{2} \rightarrow \frac{5}{2}$ transition using the correction $a_c/4 - A/2$ (a_c is the Fermi contact constant of the $1s$ electron and $A=-4493.13$ MHz is the hyperfine constant of the $1s2s\ ^3S_1$ level in ^{3}He); only for $n=5$ this factor differs slightly from 80.16 Mhz. The resulting TIS is given in Table V. The residual isotope shift (RIS) is obtained after subtraction of the NMS (see Table V). The difference between experimental RIS and calculated SMS is given in the last column of Table V. Inspection of this column indicates a systematic difference between experiment and the theoretical calculations of Kono and Hattori,[3] which is averaged to be $-6.8(25)$ MHz. A systematic difference may only be attributed to the common level in all transitions, i.e., $1s2s\ ^3S_1$. A value of 2189.6(25) MHz for the $1s2s\ ^3S_1$ SMS follows. This value is compared with other experimental data in Table VIII. Our result agrees within one standard deviation with the corrected value of de Clercq *et al.* of 2191.7(37) MHz (Refs. 17 and 23) but deviates from the result of 2202(9) MHz obtained by Bloomfield *et al.*[19] The difference may be attributed to a possible error in the experimental isotope shift of the $5\ ^3P \rightarrow 13\ ^3D$ transition (possibly a Stark shift in the $1s13d$ level) used to extract the $1s2s\ ^3S_1$ SMS in Ref. 19. This value, $-1113.1(50)$ MHz, assumed to be the SMS of the $5\ ^3P$ level differs by 11.6 MHz from the calculated value deduced from Kono and Hattori. The result of our semiempirical calculation for the $n\ ^3P$ SMS, using the value of 2189.6 MHz for the $1s2s\ ^3S_1$ SMS, all agree within the error with the extrapolated calculations of Kono and Hattori. Our value of the $1s2s\ ^3S_1$ SMS agrees well with the 2190.29 MHz deduced from Drake[25] and confirms the mass dependence of $\langle \mathbf{p}_1 \cdot \mathbf{p}_2 \rangle$ (see also Table VIII). This good agreement between experiment and

TABLE VIII. Experimental and theoretical values of the specific mass shift (SMS) between ^{3}He and ^{4}He (in MHz).

	SMS	
Level	Theor.	Expt.
$1s2s\ ^3S_1$	2196.400(1)[a]	2189.6(25)[b]
	2196.400(1)[c]	2191.7(37)[d]
	2190.29(1)[e]	2201.9(90)[f]
$1s5p\ ^3P$	−1124.71(1)[a]	−1127.7(47)[b]
	−1079(90)[c]	−1113.1(50)[f]
$1s6p\ ^3P$	−644.67(1)[a]	−645.3(56)[b]
$1s8p\ ^3P$	−268.87(1)[a]	−270.0(39)[b]

[a]Reference 3.
[b]This work.
[c]Reference 27.
[d]References 17 and 23.
[e]Reference 25.
[f]Reference 19.

theory shows that relativistic contributions to the mass shift[25,17] cannot contribute more than a few MHz.

V. CONCLUSIONS

The results presented in this work demonstrate the high accuracy and sensitivity of laser–atomic-beam experiments in the study of highly excited states of helium. The combination of an intense metastable source and a tunable cw uv laser in the wavelength region 260–300 nm has resulted in accurate measurements of ^{4}He fine-structure splittings ($n=5$–18), ^{3}He hyperfine-structure splitting ($n=5$–79), and isotope shifts between ^{3}He and ^{4}He ($n=5$–79). No field-induced line broadening or splitting was observed (linewidth 15 MHz FWHM) up to $n=100$.

For $n<20$ the fine and hyperfine splittings agree with theory based on a single $1snp$ configuration. For $n>20$ deviations occur in the hyperfine-structure energies which are shown to be due to n-mixing effects. In a three-channel two-limit MQDT model for the $F=\frac{1}{2}$ and $F=\frac{3}{2}$ series these effects are accurately accounted for. Effects of n mixing are therefore already important at the MHz level for $n=20$ although the separation between the n and $n+1$ configuration is 750 GHz. The reason is the large value of the hyperfine-structure constant ($a_c=-9$ GHz) as well as the large quantum-defect difference between ^1P and ^3P (0.08). As a result the first anticrossing between levels of neighboring $1snp$ Rydberg levels is predicted already at $n=91$. This is lower than recently observed and analyzed in the $5sns$ series of ^{87}Sr (Ref. 24) (at $n=109$).

The experimental value for the isotope shift for $n=5$–79 is in excellent agreement with sophisticated variational calculations and confirms the mass dependence of the mass polarization for the $1s2s\ ^3S_1$ level calculated by Drake.[25]

Note added. In Sec. IV relativistic corrections to the specific mass shift SMS of the $1s2s\ ^3S_1$ level were estimated to be smaller than the experimental accuracy of 2.5 MHz. Recently Drake[35] calculated this contribution to be -1.206 MHz. This confirms our assumption and reduces the theoretical value of SMS to 2189.08 MHz, in slightly better agreement with experiment.

ACKNOWLEDGMENTS

The authors would like to thank Erwin Bente, Jacques Bouma, Robert de Graaff, and Chris Lahaye for their support with the experiments and the data analysis and Roelant van Dierendonck for suggesting the idea to calibrate the 150-MHz étalon. Odile Robaux and Mireille Aymar are gratefully acknowledged for the use of their MQDT computer code. Financial support from the Foundation for Fundamental Research on Matter (FOM) and the Netherlands Organisation for the Advancement of Research (NWO) is gratefully acknowledged.

[1]U. Fano and A. R. Pau, *Atomic Collisions and Spectra* (Academic, New York, 1986); M. Aymar, Phys. Rep. **110**, 163 (1984).
[2]W. C. Martin, Phys. Rev. A **36**, 3575 (1987).
[3]A. Kono and S. Hattori, Phys. Rev. A **34**, 1727 (1986).
[4]E. S. Chang, Phys. Rev. A **35**, 2777 (1987).
[5]J. W. Farley, K. B. MacAdam, and W. H. Wing, Phys. Rev. A **20**, 1754 (1979).
[6]T. A. Miller and S. A. Freund, Adv. Magn. Reson. **9**, 49 (1976); J. P. Descoubes, in *Physics of the One- and Two-Electron Atoms* (North-Holland, Amsterdam, 1969), p. 341; W. Wittmann, K. Tillmann, H. J. Andrä, and P. Dobberstein, Z. Phys. **257**, 279 (1972); R. D. Kaul, J. Opt. Soc. Am. **57**, 1156 (1967).
[7]C. J. Sansonetti and W. C. Martin, Phys. Rev. A **29**, 159 (1984).
[8]T. J. Sears, S. C. Foster, and A. R. W. McKellar, J. Opt. Soc. Am. B **3**, 1037 (1986); H. Gerhardt and T. W. Hänsch, Opt. Commun. **41**, 17 (1982).
[9]F. Biraben, E. de Clercq, E. Giacobino, and G. Grynberg, J. Phys. B **13**, L685 (1980).
[10]L. A. Bloomfield, H. Gerhardt, and T. W. Hänsch, J. Phys. B **16**, L89 (1983).
[11]L. A. Bloomfield, H. Gerhardt, and T. W. Hänsch, Phys. Rev. A **26**, 3716 (1982); **27**, 850 (1983).
[12]M. Andersson and L. R. Pendrill, Phys. Scr. **30**, 403 (1984).
[13]J. D. Prestage, C. E. Johnson, E. A. Hinds, and F. M. J. Pichanick, Phys. Rev. A **32**, 2712 (1985).
[14]D.-H. Yang, P. McNicholl, and H. Metcalf, Phys. Rev. A **33**, 1725 (1986).
[15]S. Runge, A. Pesnelle, M. Pendrix, D. Sevin, N. Wolffer, and G. Watel, Opt. Commun. **42**, 45 (1982).
[16]L. A. Bloomfield, H. Gerhardt, T. W. Hänsch, and S. C. Rand, Opt. Commun. **42**, 247 (1982).
[17]E. de Clercq, F. Biraben, E. Giacobino, G. Grynberg, and J. Bauche, J. Phys. B **14**, L183 (1981).
[18]D. Bloch, G. Trénec, and M. Leduc, J. Phys. B **18**, 1093 (1985).
[19]L. A. Bloomfield, H. Gerhardt, and T. W. Hänsch, Phys. Rev. A **27**, 2261 (1983).
[20]R. R. Freeman, P. F. Liao, R. Panock, and L. M. Humphrey, Phys. Rev. A **22**, 1510 (1980).
[21]H. A. Schluesser, E. N. Fortson, and H. G. Dehmelt, Phys. Rev. **187**, 5 (1969).
[22]S. D. Rosner and F. M. Pipkin, Phys. Rev. A **1**, 571 (1970).
[23]W. C. Martin and C. J. Sansonetti, Phys. Rev. A **28**, 502 (1983).
[24]J.-Q. Sun and K. T. Lu, J. Phys. B **21**, 1957 (1988).
[25]G. W. F. Drake, Nucl. Instrum. Methods Phys. Res. B **31**, 7 (1988).
[26]A. H. Wapstra and G. Audi, Nucl. Phys. A **432**, 1 (1985).
[27]Y. Accad, C. L. Pekeris, and B. Schiff, Phys. Rev. A **4**, 516 (1971).
[28]D. W. Fahey, W. F. Parks, and L. D. Schearer, J. Phys. E **13**, 381 (1980).
[29]E. R. Eliel, W. Hogervorst, K. A. H. van Leeuwen, and B. H. Post, Opt. Commun. **39**, 41 (1981).

[30]C. E. Theodosiou, At. Data Nucl. Data Tables **36**, 97 (1987).
[31]W. Vassen, E. Bente, and W. Hogervorst, J. Phys. B **20**, 2383 (1987).
[32]F. B. Dunning, A. C. H. Smith, and R. F. Stebbings, J. Phys. B **4**, 1683 (1971).
[33]P. Juncar, J. Pinard, J. Hamon, and A. Chartier, Metrologia **17**, 77 (1981).
[34]C. E. Burkhardt, R. L. Corey, W. P. Garver, J. J. Leventhal, M. Allegrini, and L. Moi, Phys. Rev. A **34**, 80 (1986).
[35]G. W. F. Drake (private communication); G. W. F. Drake and A. J. Makowski, J. Opt. Soc. Am. B **10**, 2207 (1988).